



Indole Derivatives as Organic Corrosion Inhibitors of Low Carbon Steel in HCl Medium-Experimental and Theoretical Approach

Francis Kolawole Ojo¹ · Isaiah Ajibade Adejoro² · Joseph Anireju Lori¹ · Oluwatoba Emmanuel Oyeneyin³ · Kovo Godfrey Akpomie⁴

Received: 10 March 2022 / Accepted: 8 May 2022
© The Tunisian Chemical Society and Springer Nature Switzerland AG 2022

Abstract

Corrosion remains a major problem in the manufacturing industries and the whole world at large, hence the need to control it. Organic molecules have been used in the past and recent times because they have certain advantages over inorganic molecules. Information on the use of indole derivatives as anti-corrosive agents is scanty. In this work therefore, two indole derivatives, 6-benzyl-2H-indol-2-one and 3-methylindole were investigated for their ability to provide protective coverage on the surface of low carbon steel (LCS) and serve as anti-corrosive agents. Their corrosion rates and inhibition efficiencies were determined by weight loss, gasometric, electrochemical and theoretical methods. Images of LCS in the absence of inhibitor and acid, in the presence of acid only and in the presence of acid and inhibitors were recorded with the aid of Scanning Electron Microscopy (SEM). Quantum mechanical calculations on the energies of the frontier molecular orbitals (FMOs) were performed using the density functional theory. The FMOs energies were used to calculate the reactivity descriptors which inform about the inhibition capacity of the molecules. Monte Carlo simulation was used to perform the adsorption of the molecules on the surface of Fe(110). These molecules inhibit the corrosion of LCS with inhibition efficiencies of the inhibitors increasing at lower temperature, with all the inhibitors having their highest inhibition efficiencies at 303 K and at the concentration of 10×10^{-5} M. Potentiodynamic polarisation curves revealed that both inhibitors are mixed-type inhibitors. The SEM images revealed that the surface of the low carbon steel was protected by these organic inhibitors. The activation energies (12.21–55.40 kJ/mol) and the Gibbs free energy values (– 4.51 to – 8.58 kJ/mol) obtained from the weight loss method supported a physical adsorption mechanism. The adsorption was found to obey Langmuir adsorption isotherm. All theoretical results are consistent with experimental results. These molecules could be adopted for use as anti-corrosive agents in the oil, gas and manufacturing industries.

Keywords Potentiodynamic polarisation · Langmuir adsorption isotherm · Indole derivatives · Scanning electron microscopy · Density functional theory

✉ Francis Kolawole Ojo
fktdavid2@gmail.com

✉ Oluwatoba Emmanuel Oyeneyin
oluwatoba.oyeneyin@aau.edu.ng;
emmanueltoba90@gmail.com

¹ Department of Chemical Sciences, Bingham University, Karu, Nigeria

² Department of Chemistry, University of Ibadan, Ibadan, Nigeria

³ Theoretical and Computational Chemistry Unit, Department of Chemical Sciences, Adekunle Ajasin University, Akungba-Akoko, Ondo State, Nigeria

⁴ Department of Pure and Industrial Chemistry, University of Nigeria, Nsukka, Nigeria

1 Introduction

Corrosion is a process causing serious concern for industry workers and the society at large. Its debilitating effects have resulted in loss of lives and properties, increased cost of production arising from maintaining and/or replacing worn out equipment and machine parts which come in contact with acid solutions during acidization, pickling and descaling [1]. Controlling corrosion therefore, remains sacrosanct for increased longevity of industrial machines and domestic appliances. The use of corrosion inhibitors has become popular over the pre-existing methods of corrosion control. Inorganic corrosion inhibitors are frequently used in protecting metals from acidic solutions. However, their applications

have been limited by high cost of production and toxicity [2]. Thus, the search for alternatives which are affordable and non-toxic [3]. The adsorbed inhibitors on the metal could disturb the process, either by blocking the metal surface or by changing the activation barriers of the reactions involved in corrosion [4]. Effective organic compounds are those containing hetero atoms like phosphorus, sulfur, nitrogen and oxygen [5–7]. The presence of aromatic rings and conjugated double bonds could further enhanced the corrosion inhibition potentials of these organic compounds [8]. How effective an inhibitor molecule is, in recent studies has been linked to its spatial and electronic structure with the aid of quantum chemical methods [9, 10]. These method provide in depth information into the inhibitor–surface interaction [11, 12]. The use of quantum chemical methods offers some advantages: (i) based on the molecular structure, new compounds based on the parent compound could easily be simulated and characterized [13, 14] and (ii) in terms of reactivity of the molecules under investigation, one could understand the mechanisms of action [15]. The theoretical calculations have been used solely and in conjunction with experimental methods to investigate the corrosion inhibitive potential of molecular systems [16, 17].

The use of some indole analogues as anti-corrosive agents is interesting but not much has been reported on it. Some indole derivatives have been reported for their anti-corrosive potentials, for instance, indole and 2-oxyindole [18]. Also, some indole hydrazide derivatives were reported for their anticorrosion potentials [19]. Some indole derivatives were predicted their potential to inhibit corrosion using mathematical models from theoretical chemistry simulations [20]. However, their use as corrosion inhibitors remains scanty. Here, inhibitory potentials of two indole derivatives, 6-benzyl-2H-indol-2-one and 3-methylindole (Fig. 1) on low carbon steel (LCS) were investigated via experimental and theoretical means. LCS was chosen because it is mostly used in the equipment in the oil and gas industries [21]. Hydrochloric acid was used because it is used during acid pickling in industries [22].

2 Experimental Sections

2.1 Materials Used

The molecules, 6-benzyl-2H-indol-2-one and 3-methylindole (Fig. 1) were purchased from Manchester Organics. Cylindrical rods of low carbon steel (LCS) with composition (wt%): 0.012% Ni, 0.017% Mo, 0.040% Cr, 0.168% C, 0.154% Mn, 0.207% Si, 0.008% P and Fe was used for this experiment [23]. Specimen used in the weight loss technique and hydrogen evolution method (gasometric) were cut into cylindrical rods, each of dimension 30 mm length and 1.45 mm diameter. The rods were degreased in ethanol and acetone, dried at room temperature and kept in a desiccator. Afterwards, the weight of each rod was taken with an Ohaus Pioneer™ analytical weighing balance [24]. Specimens used in the electrochemical method are cylindrical working electrodes of dimension 80 mm length and 1.45 mm (thickness). The upper part of the working electrode (4 cm) was covered with Teflon and epoxy coating, the top most end (2 cm) was left uncovered and the exposed surface (2 cm) was polished using emery papers of finer grade, degreased by washing in ethanol, cleaned in acetone, dried and stored in a desiccator.

2.2 Preparation of Solutions

The solutions, 1 M HCl were made from dilution of conc. HCl (analytical grade 98%) with distilled H₂O. The experiments were done in 1 M HCl in the presence and absence of inhibitors in the concentration range of 2×10^{-5} to 10×10^{-5} M.

2.3 Weight Loss Method (Gravimetric Method)

The weight loss experiment was carried out on the low carbon steel following the method previously described [24]. The inhibition efficiency (%I.E), degree of surface coverage

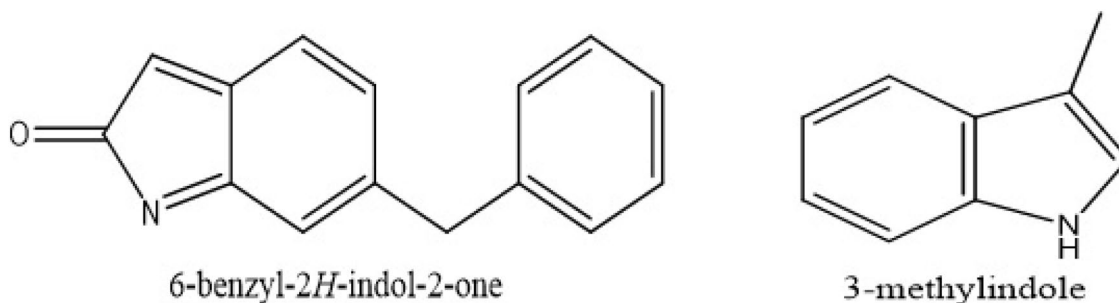


Fig. 1 Chemical structures and names of Inhibitors

(θ) and corrosion rates (C_R) were calculated from the weight loss results via Eqs. 1, 2 and 3.

$$\% I.E = \left(1 - \frac{W_1}{W_2} \right) \times 100, \quad (1)$$

$$\theta = 1 - \frac{W_1}{W_2}, \quad (2)$$

$$C_R (\text{mgh}^{-1} \text{cm}^{-2}) = W/A_t, \quad (3)$$

where W_1 and W_2 are the losses in weight (g) of LCS in the presence and absence of the inhibitor, θ is the degree of surface coverage of the inhibitor, A is the total surface area of the LCS rod (cm^2), t is the period of immersion (hours) and W is the weight loss of LCS after time (t). All the measurements were performed in triplicate and the mean value recorded.

2.4 Hydrogen Gas Evolution Method (Gasometric Method)

The gasometric method was carried out at 303 K as described earlier [25]. From the hydrogen gas liberated per minute, corrosion inhibition efficiencies were calculated by means of Eq. 4 below:

$$\% I.E = \left(1 - \frac{V_{Ht}^1}{V_{Ht}^0} \right) \times 100, \quad (4)$$

where V_{Ht}^1 and V_{Ht}^0 are the volumes of H_2 gas (cm^3) evolved at time (minutes) for inhibited and uninhibited solutions respectively.

2.5 Electrochemical Measurements

Electrochemical method was carried out at 303 K as described earlier [18]. Versa stat 4 electrochemical system at the Federal University of Technology, Akure, Nigeria was used for the test. A standard three –electrode system was used and temperature was maintained at 303 K with reference electrode (silver/silver chloride), counter electrode (platinum) and working electrode (LCS). The coupons were left to corrode freely for 30 min in the absence of external potential to acquire a stable open circuit potential (OCP) before passing external potentials from ± 0.25 V at (0.5 mVs^{-1}) in the absence and presence of different concentrations of the molecules. Each test was repeated at least two times in order to verify the reproducibility. Tafel polarization plots were generated and used to obtain different parameters (Eq. 5).

$$\% IE = \left(1 - \text{icorr}_{inh} / \text{icorr}_{free} \right) \times 100, \quad (5)$$

where $\text{icorr}(\text{free})$ and $\text{icorr}(\text{inh})$ are the corrosion current densities in the absence and presence of inhibitor, respectively. While %IE is the percentage inhibition efficiency.

2.6 Scanning Electron Microscopy (SEM)

The analysis of the morphology of the LCS surface was carried out at 303 K using scanning electron microscopy. Specimens' images were taken after exposure as follows: (a) LCS in the absence of inhibitor and acid, (b) LCS in the presence of acid only and (c) LCS in the presence of acid and inhibitors of concentration 10×10^{-5} M.

2.7 Quantum Chemical Calculations

All calculations were done with SPARTAN'14 V1.0 [26] at the B3LYP/6-31G* level of theory. The energies of the frontier molecular orbitals, FMOs (E_{HOMO} and E_{LUMO}) were obtained and used to calculate the reactivity descriptors like chemical hardness, softness and so on, as described earlier [10, 11]. The HOMO, LUMO and electrostatic potential maps were added to give insights into areas of the molecules that are acceptors and donors of electrons since corrosion inhibition mechanism is about donation of electrons from the inhibitors' orbitals to the metal's vacant d -orbitals and also back donation of electrons from the metal to the inhibitors low lying orbitals. The local reactivity indices were used to locate the sites that favour electron nucleophilic and electrophilic attacks using the Fukui analysis.

2.8 Monte Carlo Simulation

The adsorption process of the inhibitors on the surface of the metal was investigated with Monte Carlo (MC) simulation using Fe (110) surface as a template because of its well-packed structure and stability [27]. The compounds were optimized using Forcite module. Adsorption locator tool with COMPASS force field was used for the calculation in aqueous environment and also in the presence of HCl (H_3O^+ Cl^-) using simulated annealing, as was done in the experiments [28]. The total energy, E_{tot} and adsorption energy, E_{ads} (the sum of the rigid adsorption energy, E_{rig} and the deformation energy, E_{def}) were calculated in kcal/mol [29].

3 Results and Discussion

3.1 Gravimetric Analysis

Figures 2, 3, 4 and 5 show the weight loss values against different concentrations of the indole derivatives in 1 M HCl

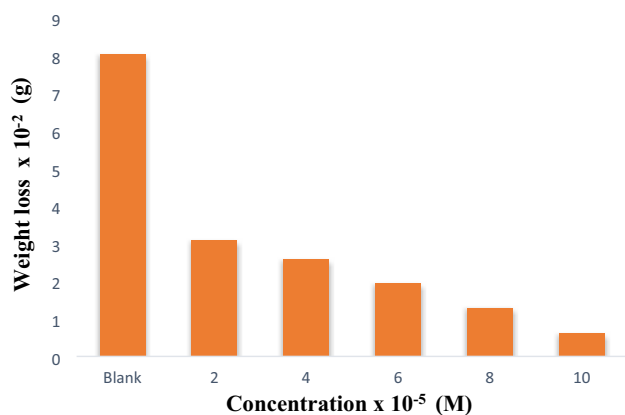


Fig. 2 Weight loss values against different concentrations of 6-benzyl-2H-indol-2-one in 1 M HCl of LCS corrosion after 8 h immersion time at 303 K

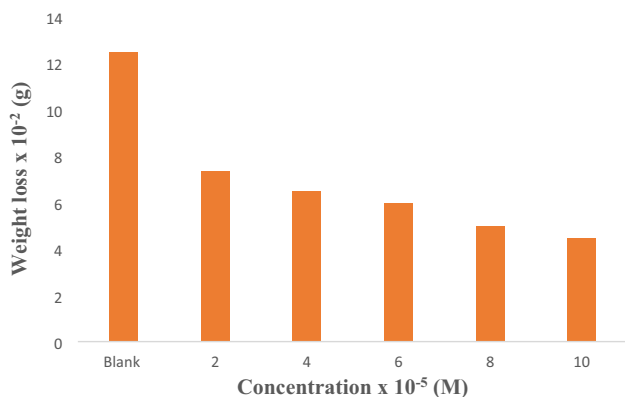


Fig. 3 Weight loss values against different concentrations of 6-benzyl-2H-indol-2-one in 1 M HCl of LCS corrosion after 8 h immersion time at 333 K

of LCS after 8 h immersion time at 303 and 333 K. Their corrosion rates (C_R) and %I.E values are recorded in Table 1. There is reduction in the C_R values with rising inhibitor concentration but increased with increase in temperature. The inhibition efficiency (%I.E) increased with rising concentration of inhibitor, getting to a peak of 92.29 and 86.32% for 6-benzyl-2H-indol-2-one and 3-methyl indole respectively. The reduction in %I.E with temperature increase is indicative of an exothermic process. Other possible causes could be from increase in solubility of the films protecting the metal surface [30], the inhibitor molecules could decompose faster at higher temperature, thereby reducing its inhibition efficacy [31] and desorption of adsorbed inhibitor molecules may occur as a result of the molecules in solution gaining more kinetic energy at higher temperature [24]. The high inhibitive performance of 6-benzyl-2H-indol-2-one when compared to 3-methylindole may be attributed to the additional unpaired electrons of oxygen atom in combination to

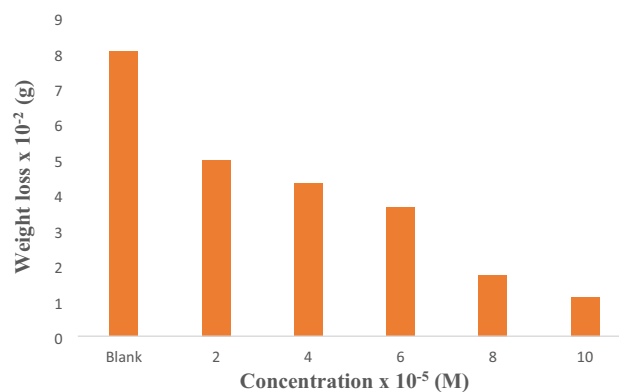


Fig. 4 Weight loss values against different concentrations of 3-methylindole in 1 M HCl of LCS corrosion after 8 h immersion time at 303 K

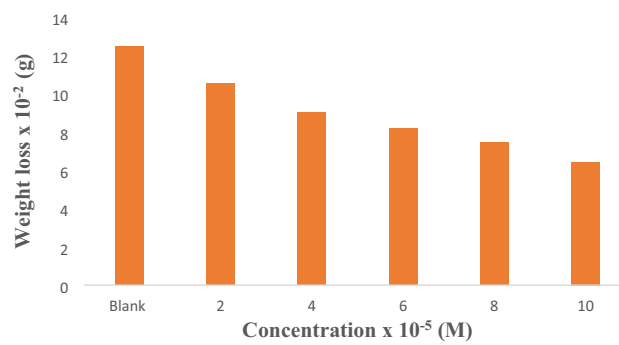


Fig. 5 Weight loss values against different concentrations of 3-methylindole in 1 M HCl of LCS corrosion after 8 h immersion time at 333 K

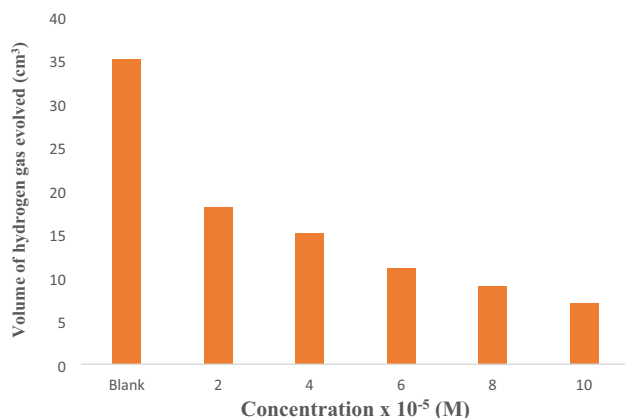
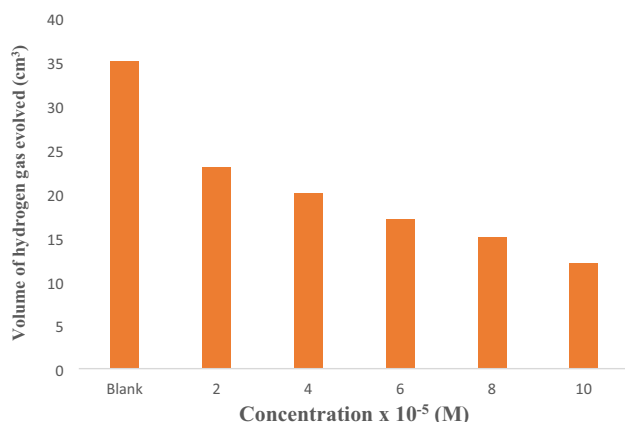
the nitrogen atom and thus enhances bonding of the inhibitor to the LCS [24].

3.2 Hydrogen Gas Evolution Measurements of Indole Derivatives

The free corrosion of LCS in 1 M HCl was described by speedy effervescence as a result of the gas (H_2) liberated. As shown in Figs. 6 and 7, the plots demonstrate the reduced deflection of H_2 liberation rate on introducing the indole derivatives into the acidic solution, signifying that the indole derivatives impedes corrosion of LCS in 1 M HCl when compared to the blank. The hydrogen gas liberation rates were seen to reduce with rising indole derivatives concentration, indicating that the inhibition was concentration dependent. The results obtained for corrosion rates and %I.E (Table 2) are similar to that of weight loss experiment. It is indicative that these inhibitors are effective with 6-benzyl-2H-indol-2-one being a more effective inhibitor than 3-methylindole.

Table 1 I.E% and corrosion rates for LCS in 1 M HCl in the presence and absence of various concentrations of indole derivatives at 303 K and 333 K via gravimetric method

Concentration (M)	Corrosion rate ($\text{Mg Cm}^{-2} \text{h}^{-1}$) $\times 10^{-3}$			Inhibition efficiency (%)				
	6-benzyl-2H-indol-2-one		3-methylindole	6-benzyl-2H-indol-2-one		3-methylindole		
	303 K	333 K	303 K	333 K	303 K	333 K	303 K	333 K
Blank	7.18	11.11	7.18	11.11	–	–	–	–
2×10^{-5}	2.76	6.56	4.45	9.39	61.57	40.92	38.06	15.43
4×10^{-5}	2.3	5.79	3.85	8.04	67.91	47.90	46.27	27.57
6×10^{-5}	1.74	5.33	3.25	7.30	75.75	52.01	54.73	34.24
8×10^{-5}	1.14	4.45	1.54	6.66	84.08	59.96	78.48	40.03
10×10^{-5}	0.55	3.99	0.98	5.73	92.29	64.06	86.32	48.39

**Fig. 6** Volume of hydrogen gas liberated against different concentrations of 6-benzyl-2H-indol-2-one in 1 M HCl of low carbon steel corrosion after 60 min reaction time at 303 K**Fig. 7** Volume of hydrogen gas liberated against different concentrations of 3-methylindole in 1 M HCl of low carbon steel corrosion after 60 min reaction time at 303 K

3.3 Adsorption Isotherm of Indole Derivatives

Langmuir isotherm is given by the equation below (Eq. 6).

$$C/\theta = 1/K_{ads} + C, \quad (6)$$

where θ is the degree of surface coverage, C (molar inhibitor concentration) and K_{ads} is the equilibrium constant. The graph of C/θ against C was linear as shown in Figs. 8 and 9 having a correlation value bigger than 0.9, with approximate unity slopes (Table 3). The results obtained established that these molecules were adsorbed on the metal's surface to shield it from corroding. The coefficients of determinant (R^2) approach unity (Table 3) when as fitted into Langmuir isotherm model, implying monolayer adsorption of the molecules. This suggest that inhibitors under study obeys Langmuir isotherm adsorption [32]. The K_{ads} values gotten from the intercept of the graph in Figs. 6 and 7 are connected to ΔG^o_{ads} via Eq. 7 [33]:

$$\Delta G^o_{ads} = -2.303RT \log (55.5 K_{ads}) \quad (7)$$

Free energy of the adsorption is represented as ΔG^o_{ads} , R =gas constant and temperature is represented as T . ΔG^o_{ads} values shown in Table 3 ranged from -8.58 to -8.25 kJ mol^{-1} for 6-benzyl-2H-indol-2-one and -6.03 to -4.51 kJ mol^{-1} for 3-methylindole. ΔG^o_{ads} values up to -20 kJ mol^{-1} usually indicates physical adsorption, the inhibition comes to play as a result of electrostatic interaction between the charged molecules and metal [4]. ΔG^o_{ads} values gotten from this research ranged from -8.58 to -4.514 kJ mol^{-1} , which agrees with the mechanism of physisorption [34].

Where

$$R = \sqrt{R^2}. \quad (8)$$

Table 2 Inhibition efficiencies (% I.E) and C_{RS} for LCS in 1 M HCl in the presence and absence of various concentrations of indole derivatives at 30 °C using hydrogen evolution technique

Concentration (M)	I.E %		Corrosion rate ($\text{cm}^3\text{min}^{-1}$)	
	6-benzyl-2H-indol-2-one	3-methyl indole	6-benzyl-2H-indol-2-one	3-methyl indole
Blank	–	–	0.58	0.58
2×10^{-5}	48.57	34.29	0.30	0.38
4×10^{-5}	57.14	42.86	0.25	0.33
6×10^{-5}	68.57	51.43	0.18	0.28
8×10^{-5}	74.29	57.14	0.15	0.25
10×10^{-5}	80.00	65.71	0.12	0.20

Fig. 8 Langmuir isotherm plot for the adsorption of 6-benzyl-2H-indol-2-one on LCS in 1 M HCl

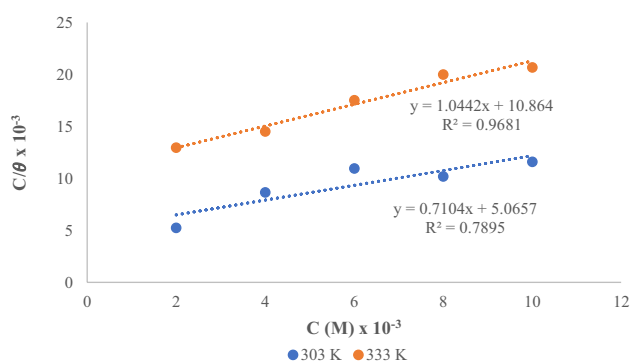
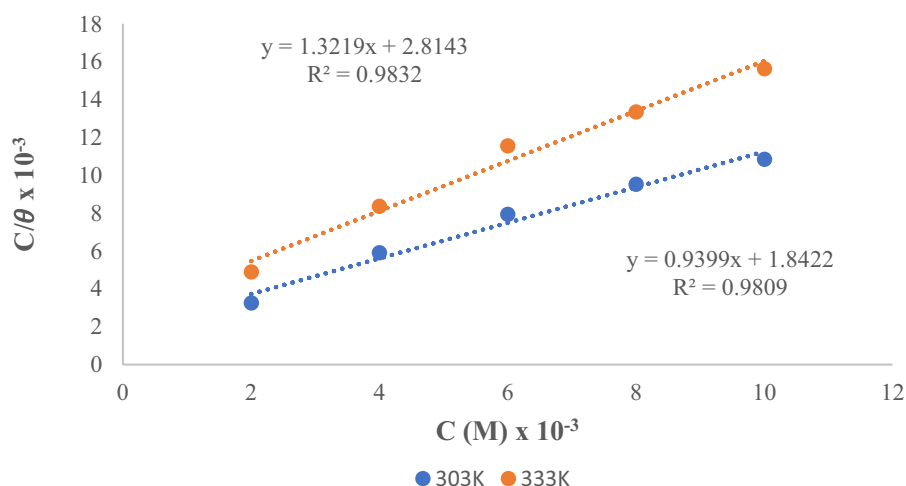


Fig. 9 Langmuir isotherm plot for the adsorption of 3-methylindole on LCS in 1 M HCl

3.4 Thermodynamic Considerations of Indole Derivatives

A greater energy of activation value (E_a) of the inhibited corrosion process when compared to an uninhibited corrosion process suggest that the adsorption mode is physisorption, while the other way round suggest chemisorption. To further show that the indole derivatives adsorbed to low carbon steel through physisorption, the E_a values were calculated using Arrhenius equation (Eq. 9).

$$\log(CR_2/CR_1) = E_a/2.303R (1/T_1 - 1/T_2), \quad (9)$$

CR_1 and CR_2 are corrosion rates at initial and final temperatures T_1 and T_2 , in that order. E_a values are recorded

Table 3 Langmuir parameters for the adsorption of indole derivatives on LCS surface

	Temp. (°C)	K_{ads}	ΔG_{ads}° (kJ/mol)	Slope	R^2	Intercept
6-benzyl-2H-indol-2-one	30	0.5428	– 8.5786	0.9399	0.9809	1.8422
	60	0.3553	– 8.2547	1.3219	0.9832	2.8143
3-methylindole	30	0.1974	– 6.0305	0.7104	0.7895	5.0657
	60	0.0920	– 4.5139	1.0442	0.9681	10.864

in Table 4. A rise in the energy of activation when indole derivatives are present as compared when they are absent and the reduction of its %I.E. with temperature rise can be understood as a sign of physisorption. With reference to Ameh et al. [35], the values of E_a should be less than 80 kJmol^{-1} for the mechanism of physisorption. With the activation energy (E_a) values as shown in Table 4 (12.20–55.42 kJmol^{-1}) for indole derivatives, it further confirms the process of physical adsorption.

An estimation of heat of adsorption was calculated via Eq. 10:

$$Q_{\text{ads}} = 2.303R [\log(\theta_2/1 - \theta_2) - \log(\theta_1/1 - \theta_1)] \times (T_1 \times T_2/T_2 - T_1) \text{ kJmol}^{-1}. \quad (10)$$

The degrees of surface coverage are represented as θ_1 and θ_2 and temperatures are represented as T_1 and T_2 . The Q_{ads} values are shown in Table 4. Calculated values of Q_{ads} using Eq. 10 ranged from -33.96 to $-53.32 \text{ kJmol}^{-1}$ for indole derivatives. The values obtained were negative suggesting that adsorption of these indole derivatives on LCS is exothermic [35].

3.5 Potentiodynamic Polarization Measurements of Indole Derivatives

Figures 10 and 11 illustrate the Tafel curves for LCS in 1 M HCl in the absence and presence of different concentrations of indole derivatives at 303 K. The strength of inhibition increases as inhibitor concentration increases. Tafel lines of inhibited systems in comparison with the uninhibited system are deflected to more negative and more positive potentials which rise with increase in the inhibitor concentration. This suggests that indole derivatives behave as mixed-type inhibitors (cathodic and anodic inhibitors) [36]. The results in Table 5 reveals that corrosion current density (i_{corr}) and corrosion rates reduce with rise in inhibitor concentration, as was observed in Migahed et al. [37]. This implies that the molecules were able to protective the surface of the mild steel, consequently reducing the number of active sites. With

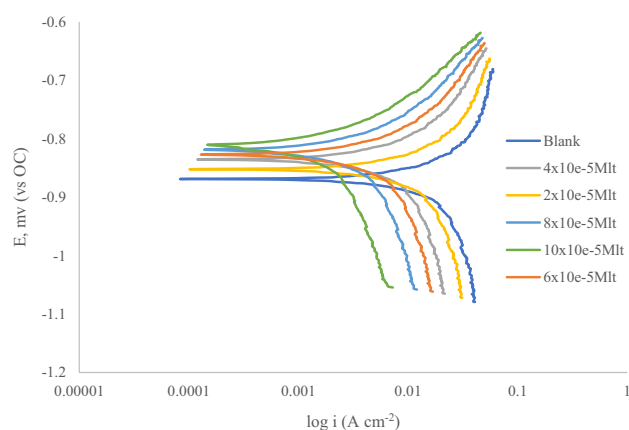


Fig. 10 Potentiodynamic polarization curves for LCS in 1 M HCl containing various concentrations of 6-benzyl-2H-indol-2-one

the greatest reduction occurring at the maximum concentration. Both slopes of the molecules were altered in relation to the blank, with the effect more felt at the anodic side, implying that though the compounds are mixed type but are predominantly anodic. The direction of increasing %I.E of the molecules are 6-benzyl-2H-indol-2-one > 3-methylindole.

3.6 Scanning electron Microscopy (SEM) of Indole Derivatives

The SEM image in Fig. 12 reveals that corrosion does not occur homogeneously over the surface of LCS in 1 M HCl solution. However, the surface is significantly protected by the indole derivatives with 6-benzyl-2H-indol-2-one being more effective than 3-methylindole in comparison to the inhibitor—free solution [38].

3.7 Quantum Chemical Study of 6-Benzyl-2H-indol-2-One and 3-Methylindole

The energies of the FMOs (E_{LUMO} and E_{HOMO}) provide information about the ability of the molecules to accept and donate electrons respectively [39, 40]. The separation energy (E_g) which connotes reactivity is the gap between

Table 4 Thermodynamic parameters for the adsorption of indole derivatives via gravimetric method

Concentration (M)	Activation energy (kJmol^{-1})		Heat of adsorption (Q_{ads}) kJ mol^{-1}	
	6-benzyl-2H-indol-2-one	3-methylindole	6-benzyl-2H-indol-2-one	3-methylindole
Blank	12.20	12.21	—	—
2×10^{-5}	24.21	20.88	− 23.45	− 33.96
4×10^{-5}	25.82	20.52	− 23.32	− 22.83
6×10^{-5}	31.31	22.63	− 29.61	− 23.56
8×10^{-5}	38.09	40.95	− 35.25	− 47.49
10×10^{-5}	55.42	49.39	− 53.26	− 53.32

Fig. 11 Potentiodynamic polarization curves for LCS in 1 M HCl containing various concentrations of 3-methylindole

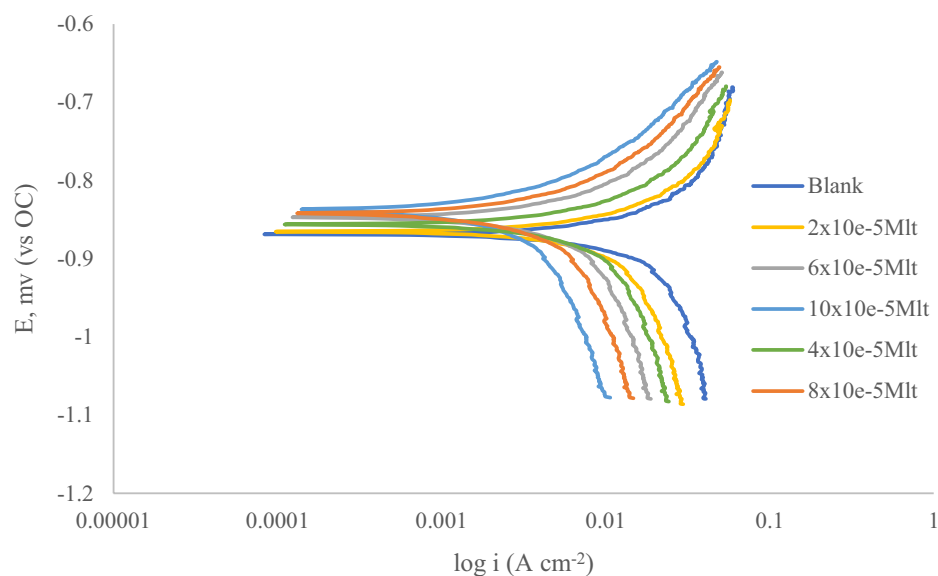


Table 5 Potentiodynamic polarization parameters for LCS in 1 M HCl with various concentrations of indole derivatives

Inhibitors	Conc. (M)	$-E_{\text{corr}}$ (mV)	β_a (V/dec)	$-\beta_c$ (V/dec)	i_{corr} (mA/cm ²)	% IE
Blank	0	435.22	0.5524	0.1220	70.948	–
6-benzyl-2H-indol-2-one	2×10^{-5}	387.28	0.1053	0.1102	19.197	72.94
	4×10^{-5}	380.62	0.1184	0.1125	15.188	78.59
	6×10^{-5}	378.11	0.1134	0.1157	12.573	82.28
	8×10^{-5}	377.01	0.1124	0.1052	8.792	87.61
	10×10^{-5}	374.38	0.1032	0.1014	4.126	94.18
3-methylindole	2×10^{-5}	421.324	0.1085	0.1219	38.521	45.71
	4×10^{-5}	403.481	0.1156	0.1196	30.355	57.22
	6×10^{-5}	389.210	0.1144	0.1282	22.751	67.93
	8×10^{-5}	381.341	0.1072	0.1154	15.193	78.59
	10×10^{-5}	376.272	0.1063	0.1121	8.437	88.11

the E_{HOMO} and E_{LUMO} . This E_g also relates to how soft or hard a molecule is. The lower the E_g the higher the reactivity towards a chemical specie. Hence, a hard molecule is less reactive than a soft molecule [41]. The extent to which an inhibitor binds to the surface of the metal improves with rising E_{HOMO} , lowering E_{LUMO} and low values of separating energy. Dipole moment (μ) is a significant quantum chemical index use in predicting the way corrosion inhibition goes. It is a way of measuring polarity in a bond and is associated with how electrons are dispersed in a molecule. Even though literature is not consistent on the usage of dipole moment predicting the way corrosion inhibition process goes, it's largely accepted that adsorption of molecules that are polar with high dipole moment values on metal surface should result to improved %I.E [42].

The quantum indices calculated (Table 6) reveal that 6-benzyl-2H-indol-2-one with E_{HOMO} and the E_{LUMO} at -6.20 eV and -3.49 eV, respectively and separation

energy of 2.71 eV clearly makes it a better corrosion inhibitor with higher reactivity toward the metal surface than 3-methylindole with E_{HOMO} and E_{LUMO} at -5.25 eV and -0.02 eV, respectively and separation energy of 5.23 eV. The HOMO energies of both molecules were stabilized in the protonated form, indicating that the protonated forms would be more difficult to donate electrons, this may be due to the lock-up of the non-bonding electrons on the nitrogen atoms. The electron affinity on the other hand increased in the protonated form. The energy band gap was also stabilized in the protonated form because of increased electron affinity. Furthermore global chemical hardness (η) and global softness (σ) were calculated, the principle of hard and soft acids and bases predicts that hard acids favours co-ordinating to hard bases or soft acids favours co-ordinating to soft bases [30]. High $E_{\text{HOMO}}-E_{\text{LUMO}}$ gap are often related to hard molecules while a low $E_{\text{HOMO}}-E_{\text{LUMO}}$ gap are related to soft molecules. On the other hand, metal e.g. low carbon

Fig. 12 SEM characteristics of the LCS in 1.0 M HCl in **a** LCS in the absence of inhibitor and acid, **b** LCS in the presence of 6-benzyl-2H-indol-2-one and acid, **c** LCS in the presence of 3-methylindole and acid **d** LCS in the presence of acid only

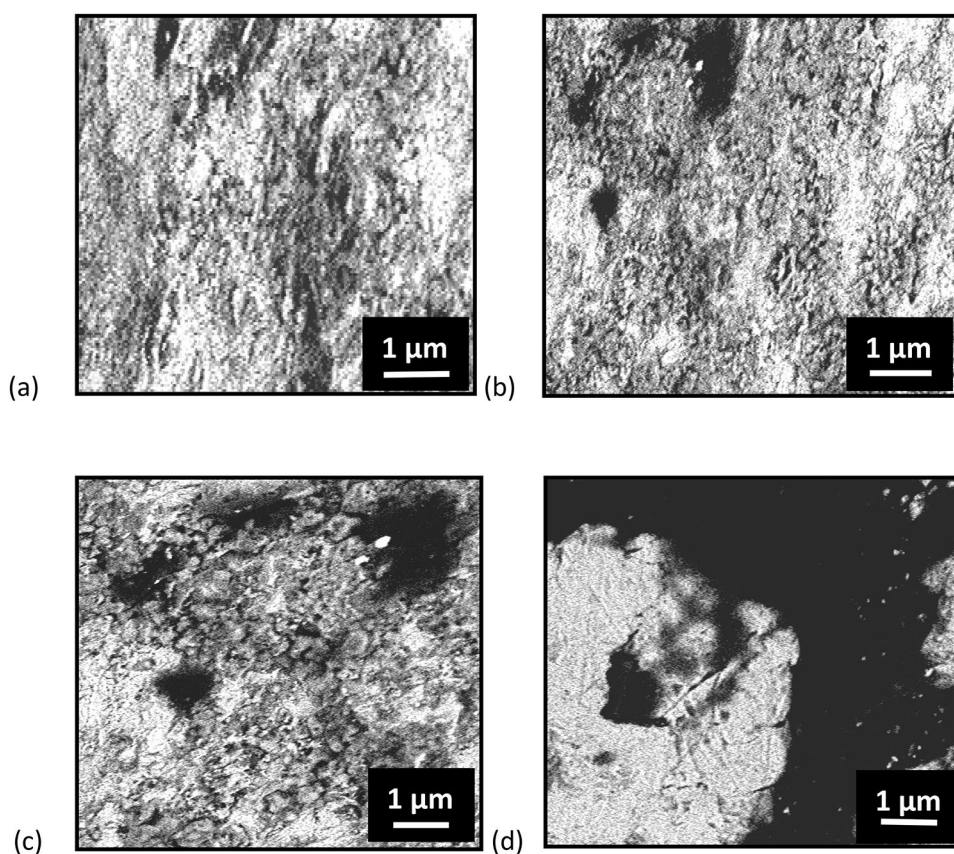


Table 6 Quantum chemical parameters of indole derivatives using DFT method

Molecules	E_{HOMO} (eV)	E_{LUMO} (eV)	E_g (eV)	I (eV)	A (eV)	η (eV)	σ (eV ⁻¹)	μ (D)
6-benzyl-2H-indol-2-one	- 6.20	- 3.49	2.71	6.20	3.49	1.36	0.738	6.44
Protonated 6-benzyl-2H-indol-2-one	- 9.40	- 7.93	1.47	9.40	7.93	0.74	1.361	5.83
3-methylindole	- 5.25	- 0.02	5.23	5.25	0.02	2.62	0.382	2.05
Protonated 3-methylindole	- 10.73	- 5.41	5.32	10.73	5.41	2.66	0.375	4.74

$$E_g = E_{\text{LUMO}} - E_{\text{HOMO}}, I = -E_{\text{HOMO}}, A = -E_{\text{LUMO}}, \eta = E_g/2, \sigma = 1/\eta, \Delta N = (\chi_{\text{Fe}} - \chi_{\text{inh}})/2(\eta_{\text{Fe}} + \eta_{\text{inh}})$$

steel are categorized under soft acids. So, soft base molecules are the most effective for metals in inhibiting corrosion [43]. The dipole moment of 6-benzyl-2H-indol-2-one (6.44 D) is well above that of 3-methylindole (2.05 D), thus further enhancing its effectiveness towards inhibiting corrosion process of LCS in acidic solution. So, 6-benzyl-2H-indol-2-one is considered to have a better corrosion inhibition efficiency than 3-methylindole judging from its values of lower energy gap, lower hardness and higher softness [4, 44].

The optimized structures of the molecules, alongside their HOMO and LUMO maps are presented in Figs. 13 and 14. The HOMO map of 6-benzyl-2H-indol-2-one is located on the phenyl and indole rings, leaving out the carbonyl group, the LUMO map is also on the phenyl and indole rings including the carbonyl group (Fig. 13).

The HOMO map of 3-methylindole is on almost all the parts of the molecule while the LUMO map excluded the methyl group (Fig. 14). This is indicative that the molecules can donate electrons to vacant orbitals of the metal and also accept electrons via back donation.

3.8 Fukui Function Analysis

The Mulliken charges for the cationic, anionic and neutral species were used to calculate the dual descriptors F_k^+ and F_k^- . The highest value of f_k^+ for 6-benzyl-2H-indol-2-one (Table 7) is 0.015 located at C11, also the highest value of its f_k^- is 0.018 located at C11, with a Δf_k of - 0.003, indicating that the site favours electrophilic attack. In the same vein, for 3-methylindole (Table 8), the highest value of f_k^+ is at C5 (0.007) with Δf_k of 0.026,

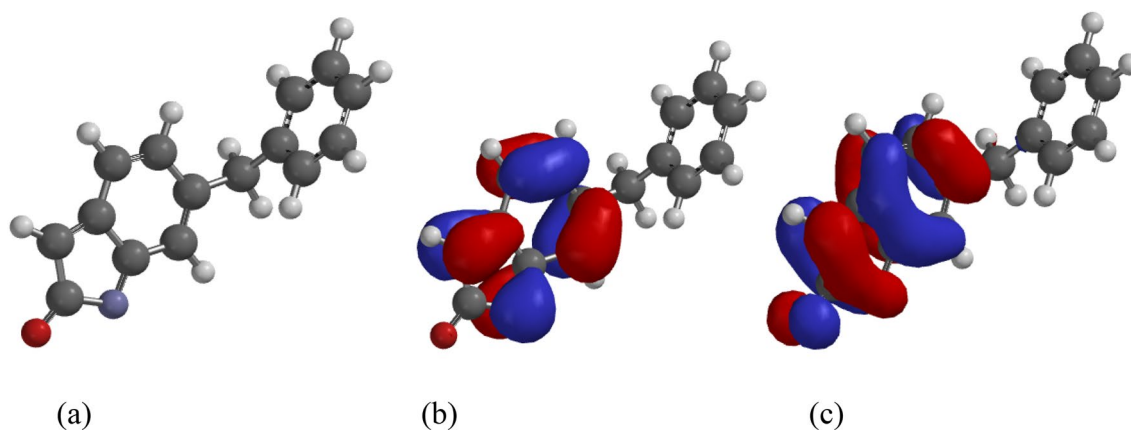


Fig. 13 **a** Optimized structure, **b** HOMO map and **c** LUMO map of 6-benzyl-2H-indol-2-one

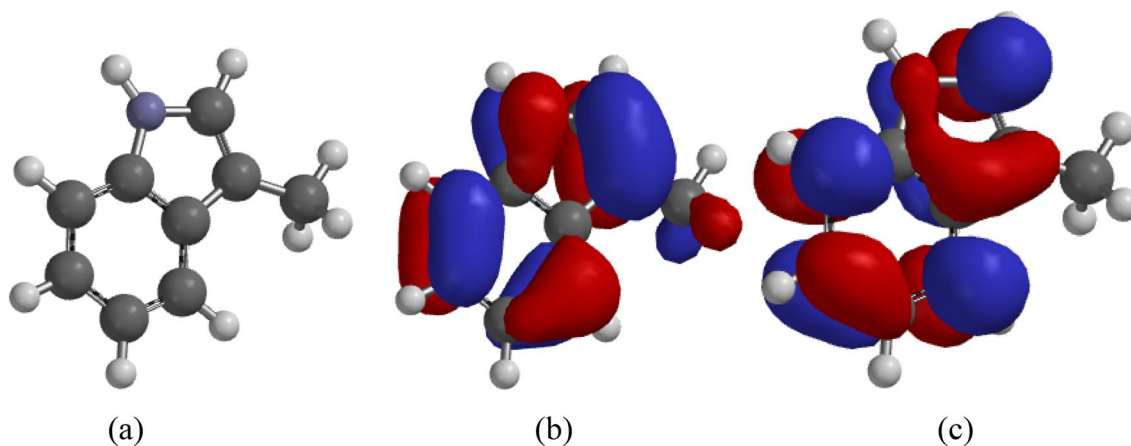


Fig. 14 **a** Optimized structure, **b** HOMO map and **c** LUMO map of 3-methylindole

indicating that the site favours nucleophilic attack. The highest value of f_k^- is at C9 (0.018) with Δf_k of -0.008 , indicating that the site favours electrophilic attack [11].

3.9 Monte Carlo Analysis

The adsorption of the molecules on the surface of Fe(110) was done and the energies calculated from it are presented (Table 9). The E_{tot} suggests that 6-benzyl-2H-indol-2-one (-1.31×10^{-4} kcal/mol) is more stabilized thermodynamically than 3-methylindole (-1.21×10^{-4} kcal/mol), this was confirmed by the lower E_{ads} of 6-benzyl-2H-indol-2-one (-1.69×10^{-4} kcal/mol) than that of 3-methylindole (-1.61×10^{-4} kcal/mol).

Low E_{ads} is necessary for strong adsorption of the molecules on the metal surface [27]. The surface covered by the inhibitors are shown in Fig. 15, the compound are almost parallel to the iron plane, providing good coverage to the surface by displacing water molecules. This is indicative that they interact with the metal surface via covalent and non-bonded interactions [45].

4 Conclusions

- i. Indole derivatives studied are effective corrosion inhibitor of LCS in 1 M HCl.

Table 7 Mulliken atomic charges of non-hydrogen atoms of 6-benzyl-2H-indol-2-one and their Fukui functions

6-benzyl-2H-indol-2-one	$q_k(N+1)$	$q_k(N)$	$q_k(N-1)$	f_k^+	f_k^-	Δf_k
N0	-0.619	-0.540	-0.443	-0.079	-0.097	0.018
C1	0.488	0.540	0.553	-0.052	-0.013	-0.039
C2	-0.320	-0.276	-0.192	-0.044	-0.084	0.04
C3	0.155	0.159	0.158	-0.004	0.001	-0.005
C4	-0.207	-0.155	-0.117	-0.052	-0.038	-0.014
C5	-0.207	-0.170	-0.170	-0.037	0	-0.037
C6	0.171	0.191	0.177	-0.02	0.014	-0.034
C7	-0.276	-0.235	-0.142	-0.041	-0.093	0.052
C8	0.266	0.304	0.301	-0.038	0.003	-0.041
O9	-0.573	-0.421	-0.336	-0.152	-0.085	-0.067
C10	-0.435	-0.444	-0.445	0.009	0.001	0.008
C11	0.188	0.173	0.155	0.015	0.018	-0.003
C12	-0.196	-0.195	-0.158	-0.001	-0.037	0.036
C13	-0.128	-0.125	-0.120	-0.003	-0.005	0.002
C14	-0.136	-0.129	-0.110	-0.007	-0.019	0.012
C15	-0.133	-0.127	-0.114	-0.006	-0.013	0.007
C16	-0.175	-0.175	-0.182	0	0.007	-0.007

$q_k(N+1)$, $q_k(N)$ and $q_k(N-1)$ are charges for anionic, neutral and cationic species respectively. F_k^+ (the difference between $q_k(N+1)$ and $q_k(N)$), f_k^- (the difference between $q_k(N)$ and $q_k(N-1)$), and Δf_k are the sites of nucleophilic attack, electrophilic attack and the dual descriptor respectively

Table 8 Mulliken atomic charges of non-hydrogen atoms of 3-methylindole and their Fukui functions

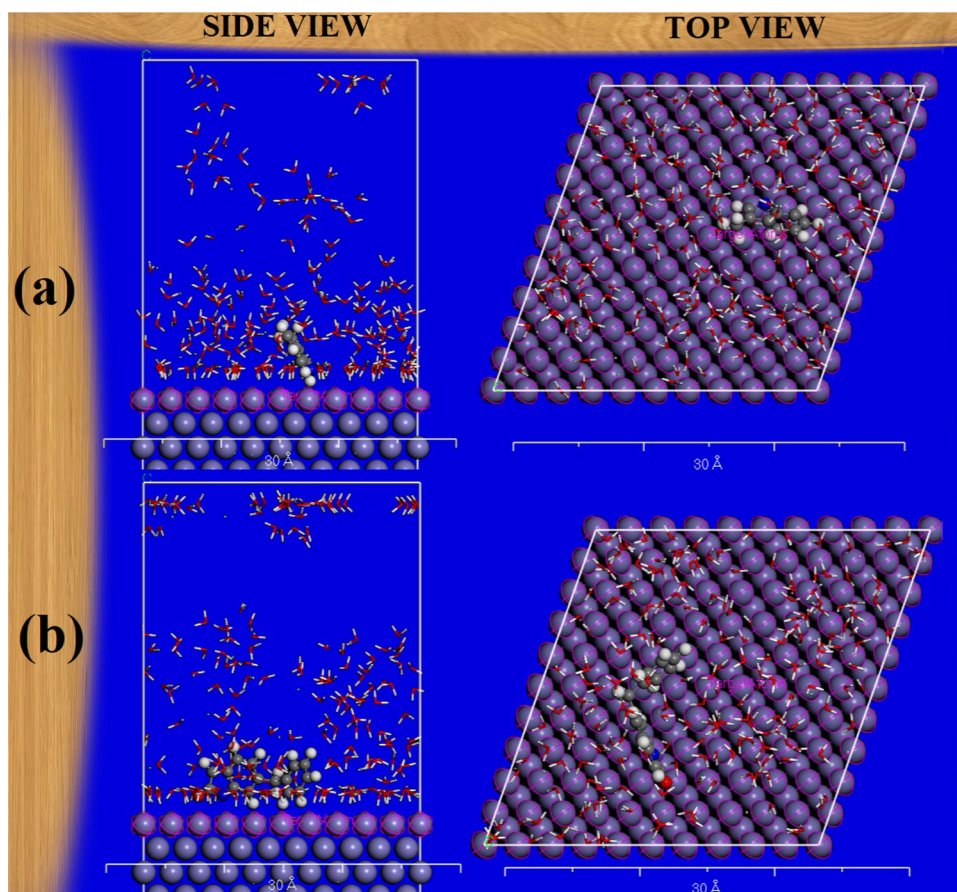
3-methylindole	$q_k(N+1)$	$q_k(N)$	$q_k(N-1)$	f_k^+	f_k^-	Δf_k
N0	-0.698	-0.690	-0.625	-0.008	-0.065	0.057
C1	-0.089	-0.005	0.106	-0.084	-0.111	0.027
C2	0.059	0.087	0.089	-0.028	-0.002	-0.026
C3	0.076	0.080	0.103	-0.004	-0.023	0.019
C4	-0.286	-0.209	-0.153	-0.077	-0.056	-0.021
C5	-0.132	-0.139	-0.120	0.007	-0.019	0.026
C6	-0.183	-0.152	-0.118	-0.031	-0.034	0.003
C7	-0.253	-0.164	-0.132	-0.089	-0.032	-0.057
C8	0.307	0.313	0.312	-0.006	0.001	-0.007
C9	-0.517	-0.527	-0.545	0.01	0.018	-0.008

Table 9 Monte Carlo simulation results of 6-benzyl-2H-indol-2-one and 3-methylindole on Fe (110) surface (all energies are in kcal/mol)

System	E_{tot}	E_{ads}	E_{rig}	E_{def}
Fe(110)-6-benzyl-2H-indol-2-one	-13,051.49	-16,901.03	-13,248.59	-3652.44
Fe(110)-3-methylindole	-12,149.36	-16,091.84	-12,457.32	-3634.52

- ii. %I.E values rises with rise in inhibitor concentration and drops with temperature increase.
- iii. The mode of adsorption of these inhibitors obeys Langmuir adsorption isotherm.
- iv. ΔG_{ads}^o values gotten (-8.58 to -4.514 kJmol⁻¹), which supports the mechanism of physisorption.
- v. The E_a values ranged from 12.20 to 55.42 kJ/mol, which also agrees with the mechanism of physisorption.

Fig. 15 Adsorption of **a** 3-methylindole, **b** 6-benzyl-2H-indol-2-one on Fe(110) surface



- vi. Theoretical results agree well with the experimental results.
- vii. These molecules could be used as anti-corrosive agents in industrial sectors.

Declarations

Conflict of interest On behalf of all authors, the corresponding author states that there is no conflict of interest.

References

- Verma C, Quraishi A, Ebenso EE (2018) Microwave and ultrasound irradiations for the synthesis of environmentally sustainable corrosion inhibitors: an overview. *Sus Chem Pharm* 10:134–147. <https://doi.org/10.1016/j.scp.2018.11.001>
- Finšgar M, Jackson J (2014) Application of corrosion inhibitors for steels in acidic media for the oil and gas industry: a review. *Corros Sci* 86:17–41. <https://doi.org/10.1016/j.corsci.2014.04.044>
- Kooliyat R, Kakkassery JT, Raphael VP, Cheruvathur SV, Paulson BM (2019) Gravimetric corrosion inhibition investigations of schiff base derived from 5,5-dimethyl-1,3-cyclohexanedione and 2-aminophenol on mild steel in 1 M HCl and 0.5 M H₂SO₄. *Int J Electrochem* 2019:1–13. <https://doi.org/10.1155/2019/1094148>
- Ebenso EE, Arslan T, Kandemirli F, Love I, Ogretir C, Saracoglu M, Umoren SA (2010) Theoretical studies of some sulphonamides as corrosion inhibitors for mild steel in acidic medium. *Int J Quan Chem* 110:2614–2636. <https://doi.org/10.1002/qua.22430>
- Barouni K, Kassale A, Albourine A, Jbara O, Hammouti B, Bazzi L (2014) Amino acids as corrosion inhibitors for copper in nitric acid medium: experimental and theoretical study. *J Mater Environ Sci* 5:456–463
- Odewole OA, Ibeji CU, Oluwasola HO, Oyeyeyin OE, Akpomie KG, Ugwu CM, Ugwu CG, Bakare TE (2021) Synthesis and anti-corrosive potential of Schiff bases derived 4-nitrocinnamaldehyde for mild steel in HCl medium: experimental and DFT studies. *J Molec Struct* 1223:129214. <https://doi.org/10.1016/j.molstruc.2020.129214>
- Oyeyeyin OE, Obadawo BS, Ojo FK, Akerele DD, Akintemi EO, Ejelonu BC, Ipinloju N (2020) Experimental and theoretical study on the corrosion inhibitive potentials of schiff base of aniline and salicylaldehyde on mild steel in 0.5M HCl. *Adv J Chem Sect B* 2(4):197–208. <https://doi.org/10.33945/SAMI/AJCB.2020.4>
- Adejoro IA, Ojo FK, Lori JA (2016) Theoretical study of the efficiency of some nitro benzenamine derivatives in acidic medium to serve as excellent organic corrosion inhibitors of mild steel. *Int Res J Pure Appl Chem* 10:1–10. <https://doi.org/10.9734/IRJPAC/2016/20772>
- Oyeyeyin OE (2017) Structural and solvent dependence of the electronic properties and corrosion inhibitive potentials of 1,3,4-thiadiazole and Its substituted derivatives—a theoretical investigation. *Phys Sci Int J* 16:1–8. <https://doi.org/10.9734/psij/2017/36555>

10. Oyeyeyin O, Akerele D, Ojo N, Oderinlo O (2021) Corrosion inhibitive potentials of some 2H-1-benzopyran-2-one derivatives- DFT calculations. *Bioint Res Appl Chem* 11(6):13968–13981. <https://doi.org/10.33263/BRIAC116.1396813981>
11. Oyeyeyin OE, Ojo ND, Ipinloju N, James AC, Agbaffa EB (2022) Investigation of corrosion inhibition potentials of some aminopyridine schiff bases using density functional theory and Monte Carlo simulation. *Chem Afr* 5:319–332. <https://doi.org/10.1007/s42250-021-00304-1>
12. Mohamed MEB, Taha KK (2015) Computational simulation of the molecular structure of benzimidazole and substituted benzimidazoles as corrosion inhibitors for brass in perchloric acid. *Am J Res Comm* 3:143–152
13. Gece G (2008) The use of quantum chemical methods in corrosion inhibitor studies. *Corr Sci* 50:2981–2992. <https://doi.org/10.1016/j.corsci.2008.08.043>
14. Amoko JS, Akinyele OF, Oyeyeyin OE, Olayanju SD (2021) Corrosion inhibitive potentials of (E)-5-((4-Benzoylphenyl)Diazenyl)-2-hydroxybenzoic acid on mild steel surface in 0.5 M HCl- experimental and DFT calculations. *J Turk Chem Soc Sect A Chem* 8(1):345–364. <https://doi.org/10.18596/jotcsa.821488>
15. Rbaa M, Dohare P, Berisha A, Dagdag O, Lakhrissi L, Galai M, Lakhrissi B, Touhami ME, Warad I, Zarrouk A (2020) New Epoxy sugar based glucose derivatives as ecofriendly corrosion inhibitors for the carbon steel in 10 M HCl: experimental and theoretical investigations. *J Alloys Comp* 833:154949. <https://doi.org/10.1016/j.jallcom.2020.154949>
16. Verma DK, Aslam R, Aslam J, Quraishi MA, Ebenso EE, Verma C (2021) Computational modeling: theoretical predictive tools for designing of potential organic corrosion inhibitors. *J Molec Struct* 1236:130294. <https://doi.org/10.1016/j.molstruc.2021.130294>
17. Obot IB, Ebenso EE, Dao DQ (2018) Editorial: discovery of novel molecules for corrosion protection using computational chemistry. *Front Chem* 6:1–3. <https://doi.org/10.1039/C6RA25094G>
18. Fouda AS, Shalabi K, Elmogazy H (2014) Corrosion inhibition of α -brass in HNO_3 by indole and 2-oxyindole. *J Mater Environ Sci* 5:1691–1702
19. Sunil D, Kumari P, Shetty P, Rao SA (2022) Indole hydrazide derivatives as potential corrosion inhibitors for mild steel in HCl acid medium: experimental study and theoretical calculations. *Trans Indian Inst Metals* 75:11–25. <https://doi.org/10.1007/s12666-021-02382-8>
20. Rodríguez JA, Cruz-Borbolla J, Arizpe-Carreón E, Gutiérrez PA (2020) Mathematical models generated for the prediction of corrosion inhibition using different theoretical chemistry simulations. *Materials* 13(24):5656. <https://doi.org/10.3390/ma13245656>
21. Li S, Zeng Z, Harris MA, Sánchez LJ, Cong H (2019) CO_2 corrosion of low carbon steel under the joint effects of concentration. *Front Mater* 6:1–17. <https://doi.org/10.3389/fmats.2019.00010>
22. Li L, Caenen P, Celis J (2008) Effect of hydrochloric acid on pickling of hot-rolled 304 stainless steel in iron chloride-based electrolytes. *Corr Sci* 50:804–810. <https://doi.org/10.1016/j.corsci.2007.09.006>
23. <https://www.totalmateria.com/articles/Art62.htm>, (n.d.)
24. Adejoro IA, Ojo FK, Obafemi SK (2015) Corrosion inhibition potentials of ampicillin for mild steel in hydrochloric acid solution. *J Taibah Univ Sci* 9:196–202. <https://doi.org/10.1016/j.jtusci.2014.10.002>
25. Ebenso EE, Ibok UJ, Umoren SA, Jackson E, Abiola OK, Oforka NC, Martinez S (2004) Corrosion inhibition studies of some plant extracts on aluminium in acidic medium. *Trans SASET* 39:117–123
26. Shao Y, Molnar LF et al SPARTAN 14', build 1.01, (2014).
27. Rahimi A, Abdouss M, Farhadian A, Guo L, Neshati J (2021) Development of a novel thermally stable inhibitor based on furfuryl alcohol for mild steel corrosion in a 15% HCl medium for acidizing application. *Indus Eng Chem Res* 60:11030–11044
28. Errahmany N, Rbaa M, Abousalem A, Tazouti A, Galai M, El Kafssauwi E, Touhami M, Lakhrissi B, Tourir R (2020) Experimental, DFT calculations and MC simulations concept of novel quinazolinone derivatives as corrosion inhibitor for mild steel in 1.0 M HCl medium. *J Mol Liq* 312:113413. <https://doi.org/10.1016/j.molliq.2020.113413>
29. Verma DK, Kaya S, Ech-chihbi E, El-Hajjaji F, Phukan MM, Alnashiri HM (2021) Investigations on some coumarin based corrosion inhibitors for mild steel in aqueous acidic medium: electrochemical, surface morphological, density functional theory and Monte Carlo simulation approach. *J Mol Liq* 329:115531. <https://doi.org/10.1016/j.molliq.2021.115531>
30. Obot IB, Obi-Egbedi NO, Umoren SA (2009) Adsorption characteristics and corrosion inhibitive properties of clotrimazole for aluminum corrosion in hydrochloric acid. *Int J Electrochem Sci* 4:863–877
31. Solmaz R (2014) Investigation of adsorption and corrosion inhibition of mild steel in hydrochloric acid solution by 5-(4-Dimethylaminobenzylidene)rhodanine. *Corr Sci* 79:169–176. <https://doi.org/10.1016/j.corsci.2013.11.001>
32. Othman MH, Al-amiery AA, Al-majedy YK, Amir A, Kadhum H, Bakar A, Sumer T (2018) Synthesis and characterization of a novel organic corrosion inhibitor for mild steel in 1 M hydrochloric acid. *Res Phys* 8:728–733. <https://doi.org/10.1016/j.rinp.2017.12.03>
33. Ebenso EE, Isabirye DA, Eddy NO (2010) Potentials of some thiosemicarbazides for the corrosion of low carbon steel in acidic medium. *Int J Mol Sci* 11:2473–2498
34. Ashassi-Sorkhabi H, Shaabani B, Seifzadeh D (2005) Effect of some pyrimidinic Schiff bases on the corrosion of low carbon steel in HCl solution. *Electrochim Acta* 50:3446–3452
35. Ameh PO, Magaji L, Salihu T (2012) Corrosion inhibition and adsorption behavior for low carbon steel by *Ficus glumosa* gum in H_2SO_4 solution. *J Pure Appl Chem* 106:100–106
36. Fouda AS, Al-sarawy AA, El-katori EE (2006) Pyrazolone derivatives as corrosion inhibitors for C-steel in hydrochloric acid solution. *Desalin* 201:1–13. <https://doi.org/10.1016/j.desal.2006.03.519>
37. Migahed MA, Azzam EMS, Morsy SMI (2009) Electrochemical behaviour of carbon steel in acid chloride solution in the presence of dodecyl cysteine hydrochloride self-assembled on gold nanoparticles. *Corr Sci* 51(8):1636–1644. <https://doi.org/10.1016/j.corsci.2009.04.010>
38. Chuan L, Bin X, Like Z, Xingwen Z, Xiao M, Shasha Z (2017) Adsorption and corrosion inhibition of mild steel in hydrochloric acid solution by S-allyl-O, O'dialkyldithiophosphates. *Res Phys* 7:3434–3443. <https://doi.org/10.1016/j.rinp.2017.09.012>
39. Ojo ND, Krause RW, Obi-Egbedi NO (2020) Electronic and non-linear optical properties of 3-(((2-substituted-4-nitrophenyl)imino)methyl)phenol. *Comput Theor Chem* 1192:1–8. <https://doi.org/10.1016/j.comptc.2020.113050>
40. Akintemi EO, Govender KK, Singh T (2022) A DFT study of the chemical reactivity properties, spectroscopy and bioactivity scores of bioactive flavonols. *Comput Theor Chem* 1210:113658. <https://doi.org/10.1016/j.comptc.2022.113658>
41. Targema M, Obi-egbedi NO, Adeoye MD (2013) Molecular structure and solvent effects on the dipole moments and polarizabilities of some aniline derivatives. *Comput Theor Chem* 1012:47–53. <https://doi.org/10.1016/j.comptc.2013.02.020>

42. Mohamed KA (2013) Quantum chemical studies and molecular modeling of the effect of polyethylene glycol as corrosion inhibitors of an aluminum surface. *Can J Chem* 91:283–291
43. Masoud MS, Awad MK, Shaker MA, El-Tahawy MMT (2010) The role of structural chemistry in the inhibitive performance of some amino pyrimidines on the corrosion of steel. *Corros Sci* 52:2387–2397. <https://doi.org/10.1016/j.corsci.2010.04.011>
44. Amoko SJ, Akinyele OF, Oyenyin OE, Olayanju DS, Aboluwoye CO (2020) Experimental and theoretical investigation of corrosion inhibitive potentials of (E)-4-hydroxy-3-[(2,4,6-tribromophenyl) diazenyl]benzaldehyde on mild steel in acidic media. *Phys Chem Res* 8:399–416. <https://doi.org/10.22036/pcr.2020.217825.1725>
45. Loto R (2018) Surface coverage and corrosion inhibition effect of *Rosmarinus officinalis* and zinc oxide on the electrochemical performance of low carbon steel in dilute acid solutions. *Results Phys* 8:172–179. <https://doi.org/10.1016/j.rinp.2017.12.003>